J Mol Model (2009) 15:9–23
DOI 10.1007/s00894-008-0366-0

ORIGINAL PAPER

Probing the interactions of the solvated electron with DNA by molecular dynamics simulations: II. bromodeoxyuridine-thymidine mismatched DNA

Tsvetan G. Gantchev · Darel J. Hunting

Received: 25 March 2008 / Accepted: 22 September 2008 / Published online: 21 October 2008

Abstract The interaction of solvated electrons (e^-_{aq}) with DNA results in various types of DNA lesions. The in vitro and in vivo sensitisation of DNA to (e^-_{aq})-induced damage is achieved by incorporation of the electron-affinity radiosensitiser bromodeoxyuridine (BUdR) in place of thymidine. However, in DNA duplexes containing single-stranded regions (bulged BUdR-DNA), the type of lesion is different and the efficiency of damage is enhanced. In particular, DNA interstrand crosslinks (ICL) form at high efficiency in bulged DNA but are not detectable in completely duplex DNA. Knowledge about the processes and interactions leading to these differences is obscure. Previously, we addressed the problem by applying molecular modelling and molecular dynamics (MD) simulations to a system of normal (BUdR·A)-DNA and a hydrated electron, where the excess electron was modelled as a localised $e^-(H_2O)_6$ anionic cluster. The goal of the present study was to apply the same MD simulation to a wobble DNA − e^-_{aq} system, containing a pyrimidine–pyrimidine mismatched base pair, BUdR·T. The results show an overall dynamic pattern similar to that of the e^-_{aq} motion around normal DNA. However, the number of configuration states when e^-_{aq} was particularly close to DNA is different. Moreover, in the (BUdR·T)-wobble DNA system, the electron frequently approaches the brominated strand, including BUdR, which was not observed with the normal (BUdR·A)-DNA. The structure and exchange of water at the sites of e^-_{aq} immobilisation near DNA were also characterised. The structural dynamics of the wobble DNA is prone to more extensive perturbations, including frequent formation of cross-strand (cs) interatomic contacts. The structural deviations correlated with e^-_{aq} approaching DNA from the major groove side, with sodium ions trapped deep in the minor groove. Altogether, the obtained results confirm and/or throw light on dynamic-structure determinants possibly responsible for the enhanced radiation damage of wobble DNA.

Keywords Bromodeoxyuridine · Electron attachment · Hydrated electron · Mismatched · Molecular dynamics · Molecular modelling · Radiosensitisation · Wobble DNA

Introduction

The solvated (hydrated) electron (e^-_{aq}) is a major species produced during water radiolysis ($G=2.8\times10^{-7}$ mol J^{-1}), and reacts with nucleobases (NB) and isolated nucleotides with bimolecular rate constants in the range of (0.9–1.7) × 10^{10} M^{-1} s^{-1} [1]. In DNA, however, the reaction rates are ~10^{7-8} M^{-1} s^{-1}. The susceptibility of NBs to be reduced and the direction of excess electron transfer (ET) along DNA follow the electron affinity (EA) of individual NBs, as predicted by reducing potentials: T,U>C>A>G [2–5].To augment the efficiency of e^-_{aq}-mediated DNA damage under irradiation, thymidine is replaced by isosteric 5-bromodeoxyuridine (BUdR). The latter is often referred to as an "electron affinic radiosensitiser" and its use has been explored in the radiation therapy of cancer. Although it is a relatively shallow electron trap (EA only 40–50 mV > EA(T) [6]), reduced BUdR efficiently sensitises DNA damage via dissociative BU^- C(5)–Br bond cleavage, ensuing the formation of a highly reactive vinyl-type U· radical. The

T. G. Gantchev (✉) · D. J. Hunting
Department of Nuclear Medicine & Radiobiology,
Faculty of Medicine, Université de Sherbrooke,
Sherbrooke, QC J1H 5N4, Canada
e-mail: tsvetan.gantchev@usherbrooke.ca

uracilyl radical is implicated in a range of subsequent reactions between NBs (e^-, H-, or hole transfer), resulting in severe DNA lesions (strand breaks and crosslinks) [7–9]. However, regardless of recent advances in the understanding of the processes of excess electron transfer along DNA, and the subsequent damage to DNA [5, 8–12], few mechanistic details concerning the primary interaction of e^-_{aq} with DNA are available.

Since the initial detection of the many isomers of e^-_{aq} [$^-(H_2O)_n$, n=6–50)] by electron paramagnetic resonance (EPR), mass spectrometry and Raman spectroscopy, there has been considerable interest in the nature of the excess electron in these clusters. The most extensive pictures of the solvent structure near the solvated electron were provided by earlier ab initio [13], quantum molecular dynamics (QMD) [14], and more recent density functional theory (DFT) and other higher order simulations [15–19]. Despite the recent progress, higher order computations, such as quantum chemical molecular dynamics (QCMD), have been successfully applied to studies of the structure, dynamics and thermodynamics of e^-_{aq} only in simple systems such as neat water or heterogeneous polar mixtures where the only additional solutes were metal ions [20, 21]. Important questions persist concerning the structure of the hydrated electron, i.e. the number of nearest water neighbours to the electron; the extent to which the solvent molecules are perturbed by the nearby charge, etc. These questions underline the debates between "cavity" and "molecular anion cluster" models. The octahedral anion structure, with OH groups pointing towards the centre of a spherical solvation cavity, known as Kevan's e^- + $6H_2O$ model, accounts reasonably well for the electron trapped in low temperature alkaline ices [22, 23]. In our previous molecular dynamics (MD) study [24] we applied this electron model to probe BUdR – DNA – e^-_{aq} interactions and the motion of the thermalised e^-_{aq} around DNA. The DNA was a normal, fully Watson-Crick base-paired duplex, where BUdR opposed adenine. We concluded that the applied MD design describes acceptably well e^-_{aq} hydrodynamics in a microheterogeneous environment (counter ions and DNA). The results provide insights into $^-(H_2O)_6$ cluster interactions, such as recruitment and dynamics of the bulk water molecules in the "second" water layer to form a two-shell, e^- + $(6+12)H_2O$ localised cavity e^- structure, the water exchange with DNA, etc. Importantly, the overall picture of DNA – e^-_{aq} interactions is consistent with a non-random approach of e^-_{aq} to only four specific bases within the major DNA groove.

We have previously shown that, in mismatched (wobble) BUdR-wDNA, e^-_{aq}-induced damage results in the efficient formation of inter-strand crosslinks (ICL) involving nucleotides that can be proximal or distant to BUdR [25–27]. The latter implies the contribution of excess electron (ET), or H-transfer processes, initiated by the primary e^-_{aq} attachment (not necessarily at the BUdR site), and followed by directed charge transfer (CT) steps. Based on our previous findings showing that the more flexible wobble DNA (w-DNA) structure is prone to frequent cross-strand (cs) inter-base atom encounters [28], our current hypothesis is that the efficient inter-strand CT in w-DNA is facilitated by the local dynamic structure of w-DNA, thus rendering such DNA segments efficient radiosensitisation targets in the radiotherapy of cancer. However, an important issue persists: are there also differences in the primary approach of e^-_{aq} to w-DNA, and/or preferences for e− attachment to BUdR, as compared with n-DNA. With these questions in mind, we have set a MD simulation experiment to probe the hydrodynamics and motion of the solvated electron around w-DNA, using the same molecular design as with n-DNA [24].

Computational methods

To permit direct comparison between the dynamics of the two systems (n-DNA versus w-DNA, plus e^-_{aq}, solvent and counter ions), the starting molecular arrangement and the applied MD protocol are essentially the same as previously described [24]. Brief details are given in the following sections.

Computations and force field

Tripos Molecular Discovery package with Sybyl 7.3–8.0 interface (Tripos, St. Louis, MO) and built-in analytical tools were used throughout this study. All molecular modelling (MM) computations applied standard Amber7_FF99 atom parameters with constant dielectric function (D=1), except that the 1–4 electrostatic term was scaled by a factor of 0.6. The particle mesh Ewald (PME) method is not accessible from Sybyl and was not applied. The AMBER7 parameterised BUdR structure was added previously to the custom-built Sybyl biopolymer monomer dictionary [28]. For further details, see [24].

Molecules

The hydrated electron model was a distance-constrained $e^-(H_2O)_6$ cluster, i.e. Kevan's octahedral cavity, single water shell structure, bearing a total charge of −1, distributed as Mulliken partial charges. In order to keep the starting MD conditions as close as possible to the previously studied n-DNA system [24], the w-DNA structure was prepared in situ, by replacement of a single nucleotide in the starting hydrated n-DNA structure with the counter ions (21 Na^+; plus 3 Na^+/Cl^- ion pairs and

$e^-(H_2O)_6$ already in place; see Fig. 1 in [24]). This was achieved by the point mutation, A(17)→T(17) in the n-DNA, 5′d(ACGAT**BU**TACGA)· d(TCGTA**A**ATCGT) sequence, to obtain a w-DNA duplex with a sequence of 5′d(ACGAT **BU**TACGA)·d(TCGTA**T**ATCGT), containing a single mismatched base pair, BU(6)·T(17) in the middle. The latter can adopt two major, interchangeable, non-Watson-Crick (wobble) conformations, generally denoted as W↑(αβ), where N3H(BU6)·O4(T17) and N3H(T17)·O2(BU6) are the H-bonded atom pairs, or W↓(βα), presenting N3H (BU6)·O2(T17) and N3H(T17)·O4(BU6) simultaneous H-bonding [28, 29]. The starting wobble configuration of the BU(6)·T(17) mismatch was chosen as W↑(αβ). The solvated periodic boundary conditions (PBC) box (38×38×49 Å), was unchanged, and contained ~2,800 TIP3P water molecules. Subsequently, the system was subjected to energy minimisations; first the w-DNA plus counter ions only (steepest descent algorithm), then the complete system (conjugated gradient algorithm). The geometry-optimised complete system potential energy was ca. -2.5×10^4 kcal/mol, to which the contribution of w-DNA was ca. −400 kcal/mol.

Molecular dynamics

MD simulations encompassed essentially the same preparative and production run stages as in [24]. First the system was subjected to one round of simulated annealing-quenching (water bath only, canonical N, T, V ensemble), followed by an unconstrained conjugated gradient geometry optimisation with or without harmonic constraints invoked. The heating phase (isobaric N, T, P ensemble) was set to 250 K in steps of 50 K. Similar to [24], this temperature was selected to correspond to the experimental conditions (glassy matrix) typically used in experiments. Total prolongation of the preparative phase was ~50 ps, thereafter the following 2,000 ps were part of the production MD and the output subjected to various analyses.

MD output

Analyses were performed using Tripos graphics and analytical tools, as outlined in [24]. Data from the history file were filled in the Dynamics-Table, together with custom-

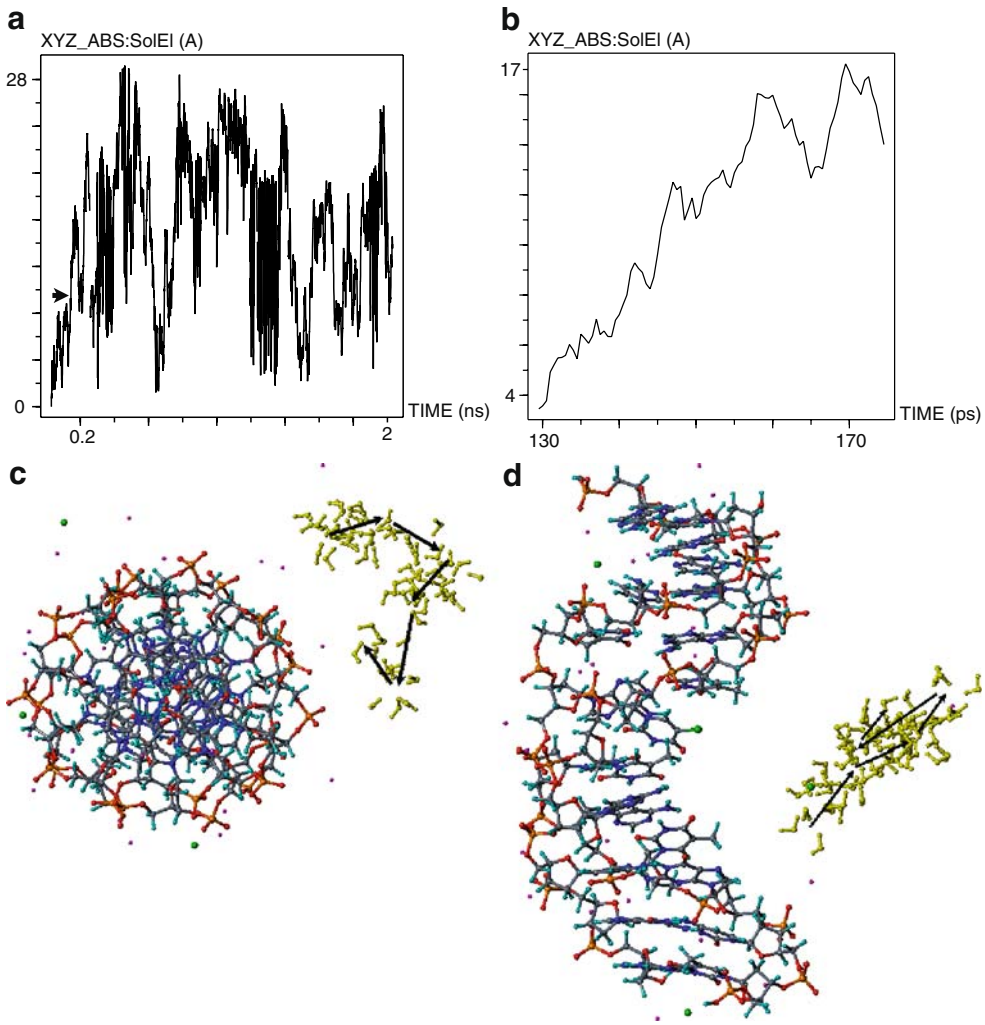

Fig. 1 **a** Absolute displacement of solvated electron (e^-_{aq}) centre of mass (XYZ_ABS:SolEl, Å) during 2 ns molecular dynamics (MD). Reference e^-_{aq} coordinates: beginning of the production run. Near-linear selections of this plot were used to calculate D(e^-_{aq}). **b** Zoomed view of XYZ_ABS trajectory section (45 ps) marked with an *arrow* in **a**. **c**,**d** Two orthogonal 3D-projections of the e^-_{aq} motion coupled with this trajectory. View along DNA Z-axis, 5′-end of the brominated strand on top (**c**), and perpendicular to DNA Z-axis (**d**). Electrons in *yellow* (*balls and sticks*). DNA and counter-ions coloured by atom type, hydration water is omitted. *Arrows* indicate direction of the e^-_{aq} dislocation

calculated system properties, accounting for ~300×4,000 tables dimension. Tripos Spreadsheet options (rows selection), coupled with a three-dimensional (3D)-molecular database built from MD frames and an interactive-graphical display were most useful. Electron hydrodynamics was characterised by the radius of gyration (RAD_{GYR}), structure deformability (mass weighted RMS-deviation, DEF_{ABS}) and diffusion coefficient, $D(e^-_{aq})$. The latter was calculated from Einstein's formula: $\left\langle [X_i(t+\Delta t) - X_i(t)]^2 \right\rangle = 6D.\Delta t$. Data were extracted from ten linear trajectory segments of the XYZ_Abs plot avoiding sites of transient immobilisation near DNA. The diffusion coefficients of water, $D(H_2O)$ (averaged over five arbitrary chosen molecules) and of a chlorine anion, $D(Cl^-)$, were calculated in a similar manner.

Results

Overview of system dynamics and hydrated electron motion

The MD output analysis performed by computing mean values, statistical variations and plotting trajectories of the global thermodynamic parameters (V, T, P), total (TE), potential (PE) and kinetic (KE) energies, solvent density, etc. showed steady values and confirmed the system thermal equilibrium (Table 1). Separately, we examined the structural dynamics of individual system components: e^-_{aq}, DNA (i.e. dictionary torsion angles), hydration water and counter ion mobility. All trajectories were smooth and fluctuations were within acceptable limits. No abnormalities, such as artificial interactions with mirror images were observed. The mean values of e^-_{aq} deformability (DEF_{ABS}) and gyration radius (R_{GYR}) are similar to the case with n-DNA [24] and the e^-_{aq} structure was always intact. The 3D movement of e^-_{aq} is represented by the 2D-trajectory of the absolute displacement (XYZ_Abs) of the $^-(H_2O)_6$ cluster centre of mass (Fig. 1a). The trajectory demonstrates an oscillation pattern: the electron traverses the space determined by the PBC, most often in a direction quasi-parallel to the DNA helix Z-axis (major groove cleft), i.e. from the O3′-end of one strand up to its O5′-end. Then, a similar path is repeated, not necessarily at the same DNA side. Apart from this longitudinal movement, shorter trajectory segments were associated with a predominant transverse motion, i.e. in a direction perpendicular to the Z-axis, or mixed. Similarly to the case with n-DNA, certain trajectory segments indicate positions of transient immobilisation close to DNA (see below). Overall, it was found that the e^-_{aq} visited most of the space around DNA, including passage over/below its ends. A zoomed view of an XYZ_Abs trajectory segment, extracted from the global trajectory is presented in Fig. 1b. The associated 3D e^-_{aq} motion (superimposed MD timeframes) is demonstrated in Fig. 1c,d. Even though large fluctuations exist, the average $D(e^-_{aq}) = 3.75 \times 10^{-9} m^2/s$ (Table 1) is practically the same as for the n-DNA-e^-_{aq} system [24], and is in the range of the reported experimental [30] and theoretical [14] estimates in pure water. Likewise, the obtained self-diffusion constant of water, $D(H_2O) = 2.1 \times 10^{-9} m^2/s$ and that of chlorine, $D(Cl^-) = 1.3 \times 10^{-9} m^2/s$ are in accordance with the estimated mobility of these species in ice (Table 1; see Discussion).

Table 1 Average thermodynamic parameters of the wobble DNA (wDNA)-hydrated electron system, calculated electron radius of gyration, deformability and diffusion coefficients of the electron, chlorine ion and water. *PE* System potential energy, *KE* system kinetic energy, *T* system temperature, *T-local*, local solvated electron temperature, R_{GYR} radius of gyration of the electron, DEF_{ABS} deformability of the electron, *D* diffusion coefficients, e_{aq}^- solvated electron

Parameter	Mean ± SD	High	Low
PE (kcal/mol)	$-(1.7 \pm 0.02) \times 10^4$	-1.6×10^4	-1.8×10^4
KE (kcal/mol)	$(6.65 \pm 0.05) \times 10^3$	6.86×10^3	6.48×10^3
T (K)	250.0±1.9	257.8	243.5
$T-local(e^-_{aq})$	255.0±60.6	256.6	86.7
$KE(e^-_{aq})$	13.7±3.2	28.2	4.6
$R_{GYR}(e^-_{aq})$ (Å)	2.28±0.07	2.52	2.06
$DEF_{ABS}(e^-_{aq})$ (mass weighted RMS, Å)	3.12±0.48	4.31	0.0
$D(e^-_{aq})$ ($m^2\ s^{-1}$)	$(3.75 \pm 2.3) \times 10^{-9}$	5.6	1.8
$D(Cl^-)$ ($m^2\ s^{-1}$)	$(1.3 \pm 0.3) \times 10^{-9}$	2.4	1.1
$D(H_2O)$ ($m^2\ s^{-1}$)	$(2.1 \pm 0.5) \times 10^{-9}$	3.2	1.5

Dynamic configurations of close distances between e^-_{aq} and w-DNA

It is presumed that charge transfer from $e^-(H_2O)_6$ to a DNA NB takes place from the closest relative positions and that the hydrated electron does not interact with DNA backbone atoms. Therefore, we examined in detail system configuration states (sites) where the electron approached and, in most cases, was immobilized by nearby DNA. These dynamic configurations encompass positions where e^-_{aq} was located predominantly on the major groove side of the DNA. Only occasionally was the electron found close to the minor groove, or interacting with backbone atoms. Figure 2 presents an integrated view of superimposed snapshots of MD configuration states selected by the rule, distance $|e^-_{aq}(H) - \text{NB atom}| < 6$ Å (electrons coloured purple). A subset, when this distance was especially short (<5 Å), was also created (electrons in yellow). The clustered ~ 139 e^-_{aq} positions (3.5% of a total of 4,000 MD configurations) usually belong to sequential states of

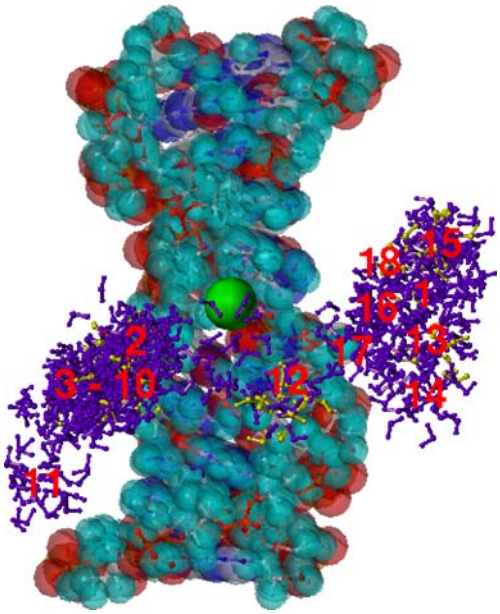

Fig. 2 Superimposed snapshots of e^-_{aq} configurations of close approach to DNA selected by the rule $|e^-_{aq}(H) - \text{NB atom}| < 6$ (*purple*), and < 5 Å (*yellow*). DNA averaged structure from 2 ns MD (*space fill*); *green sphere* van der Waal's (VdW) Br-atom; counter ions and hydration water not shown

0.5 ps each, representing a preferred residence space (site). The sites are numbered consecutively with the elapsed MD time. As it can be seen from Fig. 2, the electron tends to localise (or revisits) particular regions facing the major DNA groove, encompassing sites 2, 3–10 (left) and sites 1, 13–18 (right). In general, the electron interacts (via a set of intermediate hydration water molecules) simultaneously, or subsequently (after dynamic reorientation) with bases from both brominated and non-brominated DNA strands. Only a few sites are more distant from the most occupied, clustered localisations: the sites numbered 11 (close to the 3′-end of the brominated strand) and 12 (in the middle of the duplex), as well as several shorter-lived ones. The lifetime of most of the individual sites (excluding intermediate positions) was a few picoseconds. The most populated was cluster-site no. 15 (22 configurations, ca. 11 ps). In certain cases, e^-_{aq} closely approached DNA only for ~2 ps or less, as in cases when the distance was shorter than 5 Å. The close localisation of < 5 Å was presented by 26 dynamic states (0.7% of the total of 4,000 MD configurations). So far, the shortest $|e^-_{aq}(H) - \text{NB atom}|$ distance was identified in cluster-site no. 6, where the C5M(T7) atom is at 3.92 Å apart from an outward-pointing e^-_{aq} hydrogen atom. Table 2 summarises some characteristics of the sites of close approach. In all cases, the electron makes indirect (hydration-water-mediated) contacts with NBs, except when the closest NB atom is C5M of thymine, and most notably shows preferences to the brominated strand, including BU6. The NBs to which e^-_{aq} moves close to are: T5, BU6, T7, A8, C9 and G10 (brominated strand); and C13, G14, T15, A16 and T17 (non-brominated strand). Often, the electron was found close to tandem bases (stacks), e.g. 5′d(T5BU6); 5′d (T7A8); 5′d(G14T15), and, more rarely, in between a particular base pair, e.g. A8·T15; C9·G14. Zoomed 3D-views of several sites of close e^-_{aq}–DNA approaches are presented in the following figures. For simplicity, counter ions and bulk water are omitted, except when presenting specific hydration water molecules, which represent intermediate interactions between NB and e^-_{aq}. Figure 3a shows a single snapshot that belongs to Site-1 (Table 2), where the electron localises in the middle between the 5′d(T5BU6) base stack. This electron presents one of the rare configurations when it is near to BU6, but also interacts with an adjacent pyrimidine (T5). The site is mapped by a range of DNA – e^-_{aq} distances. However, as mentioned above, the interactions between DNA and e^-_{aq} are not direct, but are mediated by solvation water (in this case a single, shared water layer), as shown in Fig. 3b (atom space-fill presentation, for details see below). Figure 3c presents superimposed snapshots taken from clustered positions (Site-2), where e^-_{aq} is near to the 5′d(C13G14T15) nucleotide triplet from the non-brominated strand. This figure exemplifies the transient reorientation of e^-_{aq}, as it first localises close to O4 (T15) (yellow), and subsequently interacts with H41N4 (C13) (red-orange), without interacting with G14. The latter and its partner base, C9 are approached in a subsequent time interval (not shown). A set of dynamic configurations of close DNA approach, when the electron was retained for a relatively long period, flipping next to 5′d(A8C9) (brominated strand) without interacting with bases from the non-brominated strand, is shown in Fig. 3d (superimposed snapshots from Site-8).

The participation of solvent water in the interaction between DNA and e^-_{aq} is presented in the following figures. Figure 4a shows a single snapshot (Site-6) of a unique situation when e^-_{aq} localises close to three bases simultaneously; the 5′d(T7A8) doublet from the brominated strand, and G14 from the opposite strand. The relative distances are indicated. The figure also depicts the H-bonding interactions involving water molecules from the single hydration layer between e^-_{aq} and DNA. Two solvent water molecules mediate the one-step H-bridging e^-_{aq} interactions with N6H62(A8) and O6(G14), respectively. The next example of an intricate H-bonding network between e^-_{aq} and DNA is shown in Fig. 4b, which depicts a single shared hydration layer encompassing five H_2O molecules. The snapshot is again from Site-8, as in Fig. 3d. Of the five hydration water molecules, one is engaged in a one-step H-bonding involving e^-_{aq} and N7(A8); the other four participate in at least two-step H-bond bridges between e^-_{aq} and

Table 2 Sites of close contact between of e_{aq}^- and w-DNA as selected by the rule $|e_{aq}^-(H) - NB\ atom| < 6Å$ (see also Fig. 3). *NB* Nucleobase

Site ID	Elapsed time (ns)	Contact NB	Closest atoms	Distance (Å)	Population (configuration states)	Lifetime (ps)
1	0.24	T5, BU6	(T5)O4	4.97	4	2.0
			(T5)C5M	4.65		
			(BU6)O4	4.90		
2	0.30	C9, C13, G14, T15	(C9)N4H42	5.77	12	6.0
			(C13)N4H42	4.61		
			(G14)O6	5.29		
			(T15)O4	4.94		
			(T15)C5M	5.83		
3	0.32	G14	(G14)O6	5.46	3	1.5
4	0.65	T15	(T15)C5M	5.41	2	1.0
5	1.16	A8, G14	(A8)N6H61	5.50	6	3.0
			(A8)N7	5.69		
			(G14)O6	4.96		
6	1.20	T7, A8, G14, T15	(T7)C5M	3.92	11	5.5
			(A8)N6H61	4.31		
			(G14)O6	4.48		
			(T15)O4	5.04		
7	1.23	G14	(G14)O6	4.63	3	1.5
8	1.25	A8, C9	(A8)N6H61	4.54	9	4.5
			(A8)N7	4.28		
			(C9)N4H42	4.86		
9	1.27	C9, G14	(C9)N4H42	5.50	7	3.5
			(G14)O6	4.11		
10	1.30	A8, C9, G14	(A8)N6H61	5.11	5	2.5
			(C9)N4H42	4.51		
			(G14)O6	4.61		
11	1.35	C9, G10, C13	(C9)N4H42	4.35	5	2.5
			(G10)O6	5.93		
			(C13)N4H42	5.40		
12	1.41	T15	(T15)O4	5.66	4	2.0
			(T15)C5M	4.29		
13	1.43	BU6	(BU6)O4	5.30	4	2.0
14	1.45	A16	(A16)N6H61	5.24	3	1.5
15	1.60	T5, BU6, A16	(T5)O4	4.91	22	11
			(BU6)O4	4.99		
			(A16)N6H61	4.78		
			(A16)N7	5.33		
16	1.65	T5, BU6	(T5)C5M	5.52	3	1.5
			(BU6)O4	5.10		
17	1.77	BU6, T15	(BU6)Br5	5.90	4	2.0
			(T15)	5.91		
18	1.96	T17	(T17)C5M	4.91	6	3.0

A8 and C9 H-amino partners. The presence of a convoluted hydration-water H-bonding pattern interconnecting DNA and e_{aq}^- was most common in all situations in which the electron was retained longer at a given location. The strongest electron immobilisation was observed when DNA and the $^-(H_2O)_6$ cluster were separated only by a single, structured-water (H-bonded) layer. In contrast to the case of n-DNA [24], no direct (not water-mediated) interactions were identified with w-DNA.

DNA − e_{aq}^- shared hydration-water dynamics

Since the shared (transient) water layer between DNA and e_{aq}^- is likely a major factor determining the interactions, and possibly the process of ET to nucleobases per se, we examined its formation and dynamics in more detail. Previously, we have shown that the hydrated $^-(H_2O)_6$ cluster (the single-layer, cavity e_{aq}^- model) recruits about 12 structured hydration water molecules to form a tightly

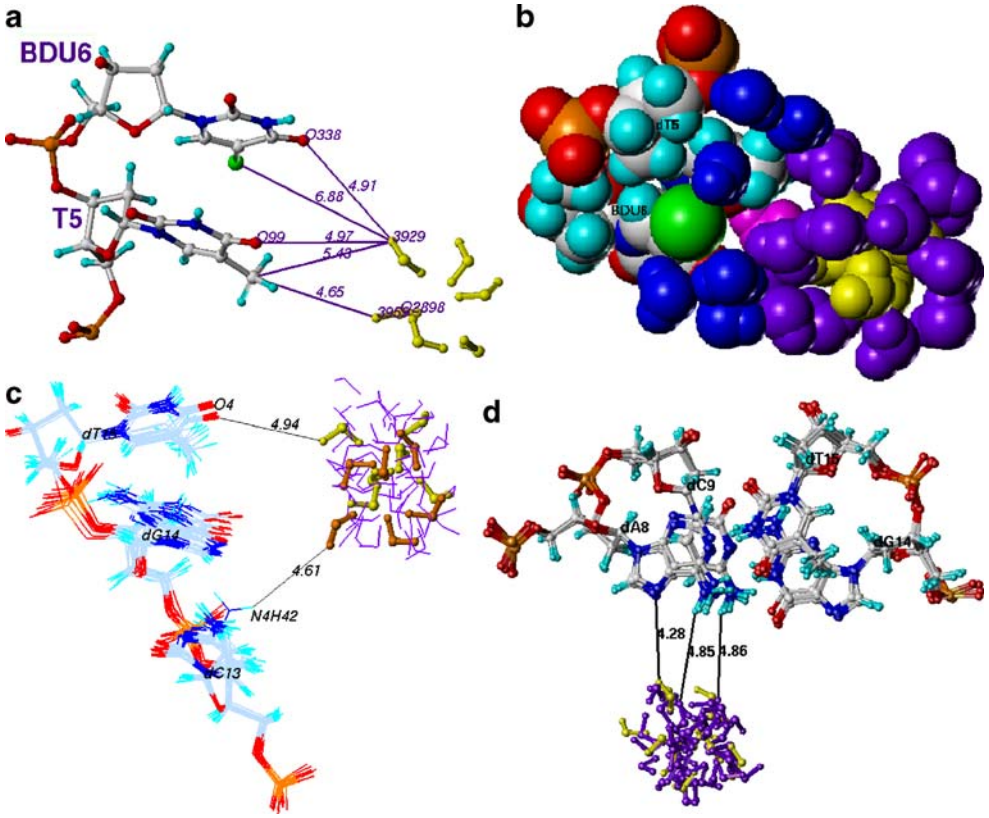

Fig. 3 **a** Example of simultaneous close interactions of e^-_{aq} (*yellow ball and stick*) with tandem bases 5′T5BDU6 (Site-1, coloured by atom types); hydration water is omitted. Distances as indicated. Notably, H(e^-_{aq}, ID3929) is close to O4(T5) and O4(BDU6), but the shortest distance is between H(ID3959) of a different e^-_{aq} water molecule and C5M(T5). **b** Space fill view of the $e^-(H_2O)_6$ (*yellow*) close-contact site with DNA shown in **a**. T5 and BDU6 coloured by atom type: *green* Br, *blue* DNA tightly bound water (6 molecules), *purple* e^-_{aq} "second shell" water (12 molecules), *magenta* shared water molecule of special interest (O-atom ID2418, see also Fig. 6). **c** Superimposed MD time-frames of the DNA segment 5′d (C13G14T15) and the e^-_{aq} cluster Site-2 (*violet*). Two e^-_{aq} localisations (*ball and stick*; *yellow and red-orange*) present subsequent reorientation and close approach first to O4(T15) and then to H41N4(C13) (distances as indicated). **d** A set of MD configurations where e^-_{aq} approaches the 5′d(A8C9)·(G14T15) base pair doublet (Site-8), but interacts only with the bases from the brominated strand. The view is along the helix axis; distances as indicated. In the configuration of closest approach, the distance to N7(A8) is 4.28 Å (*yellow*)

bound "second" shell [the e^- + (6+12)H_2O model structure; 24]. Hydrated DNA is known to have up to 12 strongly bound water molecules per nucleotide (about 4–6 per NB in the major groove). When the electron approaches DNA, the oriented water molecules of the two tightly bound layers interact and, in general, merge, while the non-H-bonded water molecules are displaced. A graphic representation of the dynamics of the formation and decay of the shared hydration shell during the process when the e^-_{aq} approaches DNA and subsequently disengages is presented in Fig. 5. The colour-coded sequential snapshots (taken from Site-2) show the water exchange and e^-_{aq} relocation during the 5 ps preceding the close approach of 4.94 Å to the O4(T15) atom, which becomes H-bonded to e^-_{aq} via a liaison H_2O molecule, and the following 5 ps of separation. This configuration of close contact is shown also in Fig. 3c, where the hydration water was omitted (A8 does not interact with e^-_{aq}). On average, about five H_2O molecules remain tightly bound in the major groove front edge (the blue cluster surrounding the A8·T15 b.p.). However, several are more mobile and exchange with the $e^-(H_2O)_6$ "second" shell. The scattered blue-coloured water cluster on the top of the yellow-coloured $e^-(H_2O)_6$ represents exchangeable molecules, bound to DNA at the moment of closest contact, but previously participating in the e^-_{aq} "second" shell water layer. During the monitored 10 ps period, a free solvent H_2O molecule traverses up to 5 Å [24], while the $e^-(H_2O)_6$ centre of mass was displaced only ca. 0.7 Å. An insight into the dynamics of bulk water recruitment in the $e^-(H_2O)_6$ "second" shell and the formation of the shared-with-DNA water-layer is presented in Fig. 6. The example shows a 20 ps trajectory segment of the e^-_{aq} centre of mass, XYZ_ABS(e^-_{aq}) (Fig. 6a); 10 ps of the build up of the configuration, Site-1 (Fig. 3a,b), and the 10 ps aftermath (e^-_{aq} in the closest approach to T4/BU6; the middle of the graph at 272 ps from the start). During the initial 10 ps, a selected H_2O molecule (ID O2418) was originally quite distant from e^-_{aq} and DNA. It was later

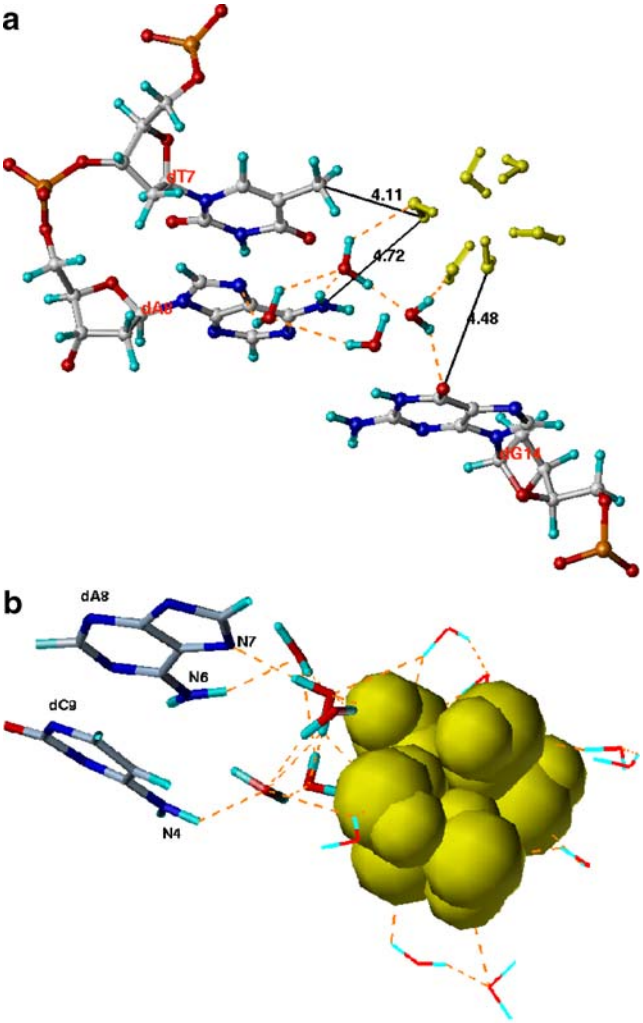

Fig. 4 H-bonding patterns formed between e^-_{aq}, hydration water and NBs in different configurations. **a** View of Site-6 where a single water layer of four molecules mediates the interaction of e^-_{aq} with two bases (A8 and G14), while only two of them form one-step H-bond bridges. Distances as indicated. *Orange dashed lines* H-bonds. C5M(T7) is the most closely approached (no intermediate water). **b** The structure of the tightly bound single water-layer between the DNA and the electron (Site-8, five H_2O molecules, *bold capped sticks*); the rest of the "second" shell waters (*lines*, in atom type colour) surround the $^-(H_2O)_6$ cluster (*yellow*, *space fill*). *Orange dashed lines* H-bonds; only one of the five molecules from the single H_2O layer mediates a single-step H-bond bridge with N7(A8); the other four present a network of two(three)-step H-bond bridges between DNA/ e^-_{aq} partner atoms

recruited into the "second" $e^-(H_2O)_6$ shell for about 5 ps (first two minima in the distance trajectory W(O2418):SolEl (O2898), Fig. 6b). Following mutual reorientation, while the electron moved towards DNA, the water W(O2418) became shared between e^-_{aq} and DNA hydration layer (H_2O coloured magenta in Fig. 3b). This event occurred at about 272 ps (the middle minima in all graphs, Fig. 6). Thereafter, W(O2418) water remained bound to both O4(T5) and O4(BU6) atoms and resided in this state for about 6 ps (Fig. 6c). Meanwhile, the e^-_{aq} "second shell" was rearranged, as the $e^-(H_2O)_6$ centre of mass was dislocated to ~ 5 Å away from the closest contact position (Fig. 6a).

DNA dynamic conformations vs system dynamic configurations

General view

Molecular dynamics simulation of w-DNA in the presence of the $e^-(H_2O)_6$ cluster discloses transient DNA structural rearrangements, which otherwise do not exist or appear when MD was performed without $e^-(H_2O)_6$ [28]. An integral view of w-DNA structure deviations is shown in Fig. 7, where backbones of the initial and the averaged from 2ns MD DNA structures (shaded ribbons, connecting C1′ atoms) are superimposed on a single MD frame DNA configuration that includes a closely located e_{aq}^- (snapshot from the most populated Site-15). The backbone in the snapshot DNA is notably distorted at the BU(6)·T(17) site (the inward dent of the brominated strand; but less so in the averaged DNA structure). Backbone dynamic divergence in wDNAs is a known phenomenon, associated with base-stacking destabilisation and shortening of the C′–C′ distances in pyrimidine mismatches [28, 31]. Additional local deviations, however, correlate with the e_{aq}^- advance-

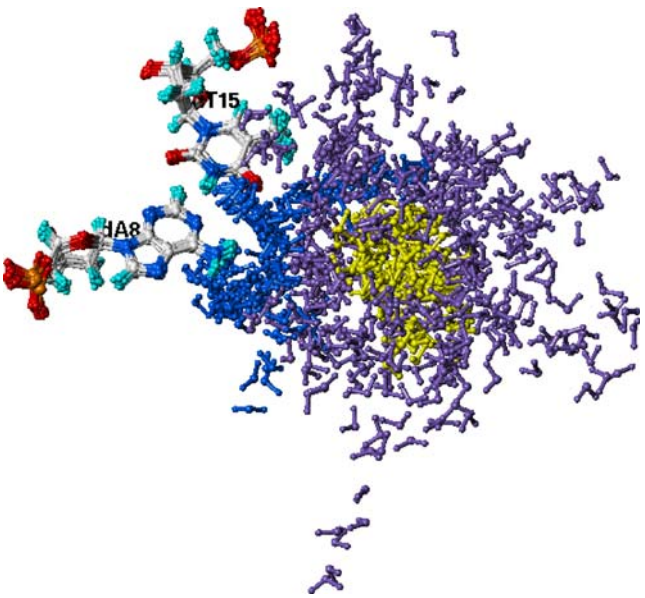

Fig. 5 Dynamics of water exchange. A set of subsequent DNA − e^-_{aq}) configurations (view along Z-axis, A8·T15 base pair only) presenting MD frames (Site-2), when the electron approaches O4(T15). The water exchange during the 5 ps before the e^-_{aq} has reached the shortest distance to T15 and the following 5 ps of disengagement is shown. Colour codes for the A8 ·T15 base pairs (by atom type): *yellow* e^-_{aq}, *blue* water molecules bounded to A8 ·T15 at the moment of closest approach, *purple* water molecules forming the e^-_{aq} 12-molecule "second shell" during the same configuration

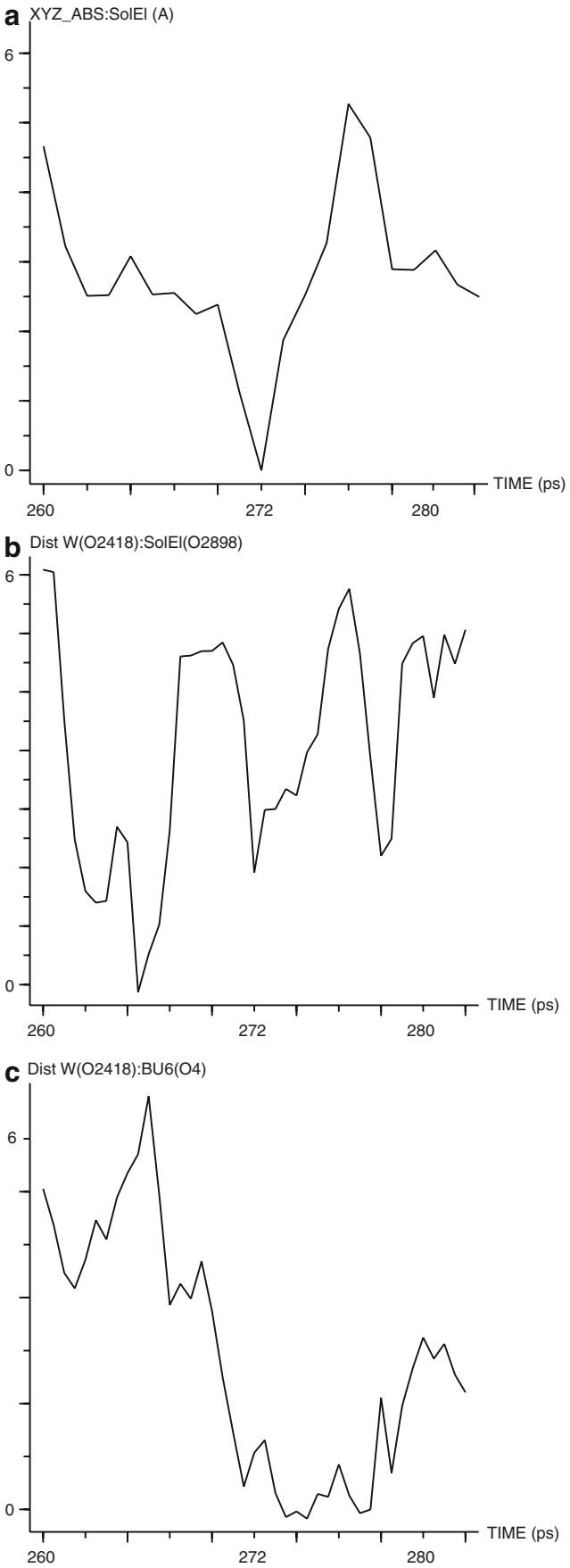

◀ **Fig. 6** Recruitment dynamics of a bulk water molecule, W(02418) (*magenta*, Fig. 3b) into the e^-_{aq} "second shell, subsequently engaged in the shared DNA – e^-_{aq} hydration layer and transiently immobilised by DNA. **a** The e^-_{aq} motion during 20 ps while approaching the short-lived site of close contact (Site-1, initial 10 ps, and 10 ps of disengagement, presented by XYZ_ABS(e^-_{aq})). Reference coordinates (zero): configuration of the closest contact with DNA, t= 272 ps (shown in Fig. 3a,b); and 20 ps distance trajectories between water O-atom (ID2418) and e^-_{aq} O-atom (ID2898) (**b**), and water O-atom (ID2418) and O4(BUdR6)-atom (**c**) (for details see text)

ment near to the central 5′d(T5BU6T7)·d(A16T17A18) triplet. The snapshot represents the configuration when $e^-(H_2O)_6$ interacts with O4(BU6), while during the previous 4–5 ps it was interacting with O4(T5). Neither of the two normal base pairs T5·A18 and T7·A16, nor the mismatched one, BU6·T17 are H-bonded, but show high buckle/stretch, shear/opening and stagger, respectively. The remaining DNA bases (not shown for simplicity) are all correctly WC-bonded. The displacement of Na^+ counter ions, initially located near the shallow cleft of the minor groove, appears to play a major role in the generation and stabilisation of the distorted w-DNA conformational states (see below). The local distortions of DNA were transient and, in general, were repaired when the electron disengaged from the DNA. The all heavy atom root mean squared deviation (RMSD) of the averaged DNA structure as

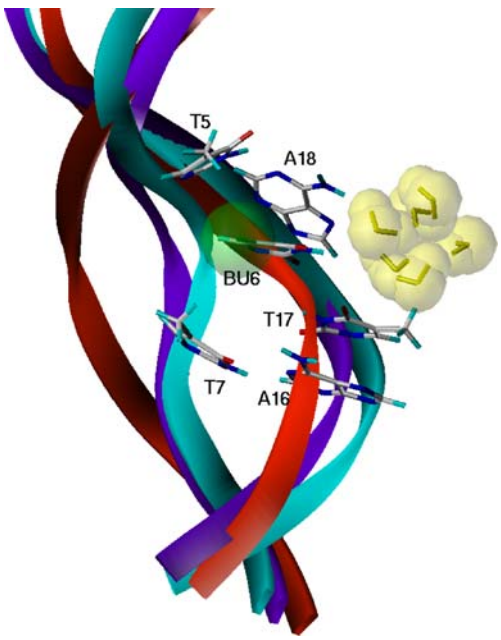

Fig. 7 DNA deformations during 2 ns MD. Starting (*red*) and averaged (*purple*) structures and a snapshot representing a configuration of close e^-_{aq} approach (*cyan*) are superimposed. *Shaded ribbons* DNA backbones, *yellow space fill VdW* e^-_{aq}, *bases in atom types*: six bases forming the central DNA triplet, *green sphere VdW* Br-atom. Note the backbone deviations at the BUdR position. None of the three base pairs is WC H-bonded. Most significant is the displacement in the BU6·T17 pair, presenting a zipper-like structure

compared with the starting B-DNA is 2.2 Å (2.0 Å and 2.5 Å for the side chain and backbone atoms, respectively). The trajectory of the mass-weighted RMS heavy atom deviation during the 2 ns simulation is shown in Fig. 8. In general, abrupt deviations coincide with positions of e_{aq}^- close contacts with DNA. The average RMSD is 2.1 Å, with fluctuations of ~1 Å, which also indicates that the global conformation remains close to that of B-DNA.

Dynamics of base-pairing, atypical inter-base (cross-strand) contacts and counter ions translocation

Table 3 lists interstrand base pair H-bonding distances and their deviations during the 2 ns MD run. The Watson-Crick H-bonding of base pairs near the DNA edges is largely preserved. As expected, G·C base pairing was more robust than A·T. In all situations, when at least one of the base-pair partners was approached by e_{aq}^-, the H-bonding of nearest neighbours was also affected (Tables 2, 3). The strongest perturbations are those of the T(5)·A(18) pair, which, apart from the frequent visits by e_{aq}^-, is an upstream 5′-neighbour of the most dynamically flexible wobble pair, BU(6)·T(17).

The presence of a BU(6)·T(17) mismatch, although accommodated in the double helix, is known to destabilise the structure due to the exchange between two alternative H-bonded conformations, denoted as W↑(αβ) and W↓(βα). General B-DNA structural effects associated with T·T and U·T mismatches include diminished base-stacking and backbone deviations, thus providing conditions for cross-strand (cs)-interactions with nearest neighbours [28, 29, 31]. From the computations presented in Table 3 it can be seen that, during the 2ns MD simulation, the wobble base pair was predominantly in the W↑(αβ) conformation, i.e. as without e_{aq}^- [28]. The distance–trajectory plots shown for two selected inter-base partner atoms are representative for the wobble pair dynamics (Fig. 9a,b). The same wDNA structure without e_{aq}^- formed several unusual cs inter-atomic contacts encompassing BU6, T17 and the two flanking base pairs, e.g. (BU6)O4^H61N6(A18) and (T7)O2^HN3(T17) (previously denoted as ρ and μ, respectively [28]). Local structure analysis in this MD study indicates additional cs inter-atomic contacts (potential cs H-bonds) that were induced during, or after, e_{aq}^- visited sites close to particular NBs: (A4)N6H62^N1(A18); (T7)O4^HN3(T15); (T7)O4^HN3(T17) and (A8)N1H^H62N6(A16) (Table 3). The distance trajectory of the most frequently formed (T7)O4^HN3(T15) shows a clear correlation with the dynamics of the e_{aq}^- approach to particular DNA sites (Fig. 9c). In different time-segments along the MD simulation, transient structural peculiarities that have been detected include a zipper-like base arrangement downstream T(5) (see Fig. 7), often accompanied by a network of bifurcated H-bonding involving triplets such as BU6:T17:T7, or A8:C9:G14 and, occasionally, a backbone pseudo-H-bond between H21N2(G14) and O4′(T15) (not shown). A typical zipper-like base arrangement (no WC H-bonding) is presented in Fig. 10 (a configuration from Site-2), where C(9)·G(14) is partially WC H-bonded (2H-instead of 3H-bonds), BU(6)·T(17) is in a full W↑(αβ) conformation, while T(7)·A(16) and A(8)·T(15) exhibit high stagger and shift and are not H-bonded. It is noteworthy that in all such distorted DNA conformations, at least one Na^+-counter ion was found trapped deep within the minor groove, so that it interacts not with phosphate oxygens, but with NB atoms. The latter is exemplified in Fig. 10, which also shows a Na^+ ion, (ID706) practically in a Van der Waal's (VdW) contact with O2(T15) and N3(A8) at distances 2.30 Å and 2.87 Å, respectively. The nearby Na^+ (ID708) is correctly located close to the PO(T7/A16) groups. The XYZ_Abs(Na706) plot (Fig. 11) demonstrates the dynamics of the penetration of Na^+ (ID706) into the minor DNA groove, coupled with the e_{aq}^- approach to DNA (Site-2, see also Fig. 10). The electron resides close to 5′d(C13G14T15) in a total of about 25 ps. While e_{aq}^- disengages from DNA, the Na706 ion slowly moves back to its usual position near the backbone PO-groups. To this end, and similar to the case with n-DNA [24], the analysis of Na^+ ions translocation indicates an average localisation at a given position of ca. 200 ps (residence time). However, in all system configurations where the e_{aq}^- advances close to NBs from the major groove side, at least one of the eight Na^+ ions facing the most frequently approached central base pairs moves in, and tends to penetrate into the minor

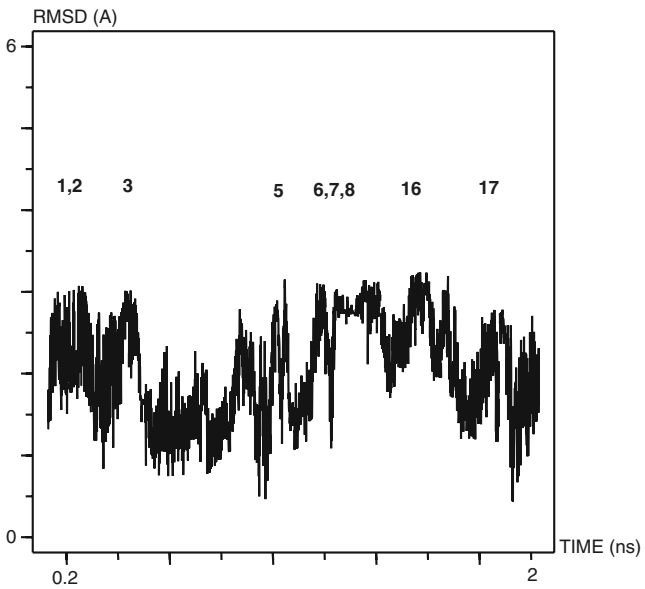

Fig. 8 Mass-weighted heavy atom root mean squared deviation (RMSD) during 2 ns trajectory in reference to the starting B-DNA structure. Close e_{aq}^-–DNA interaction sites that correlate with major upward changes are indicated. The average RMSD is 2.1±1.0 Å

Table 3 Canonical and wDNA structure deviations during 2 ns molecular dynamic (MD) simulation in the presence of e_{aq}^-: Watson-Crick (WC), wobble (wb) and cross-strand (cs) H-bonding. Single H-bonding defined by donor-acceptor inter-atomic distance ≤ 2.5 Å and proper angle. For wb and cs conformer notification see text and [28]

Inter-base contact atoms		Distance (Å)			% H-bonded	% WC or wb paired
Type	Base pair	Mean ±SD	High	Low		
WC	(G3)N2H22·O2(C20)	2.1±0.3	3.9	1.6	97.4	94.9[a]
	(G3)N1H·N3(C20)	2.0±0.3	3.8	1.7	96.9	
	(G3)O6·H41N4(C20)	2.4±0.6	4.4	1.6	81.0	81.0[b]
WC	(A4)N6H62·O4(T19)	3.7±1.2	6.2	1.7	34.3	34.3[a]
	(A4)N1·HN3(T19)	2.0±0.3	3.8	1.7	96.9	
WC	(T5)O4·H62N6(A18)	3.8±1.2	6.7	1.8	22.9	22.9[a]
	(T5)N3H·N1(A18)	2.9±1.1	5.5	1.7	64.3	
wb(α′)	(BU6)N3H·O4T17	2.6±0.4	4.4	1.8	68.7	47.2 W↑(αβ) [a]
wb(β′)	(BU6)O2·HN3T17	2.5±0.5	4.6	1.6	65.4	
wb(β″)	(BU6)N3H·O2(T17)	4.5±0.6	5.9	2.0	1.4	1.3 W↓(βα)[a]
wb(α″)	(BU6)O4·HN3(T17)	4.2±0.7	6.0	1.8	4.3	
WC	(T7)O4·H62N6(A16)	2.8±0.9	5.9	1.7	60.8	59.3[a]
	(T7)N3H·N1(A16)	2.3±0.6	4.7	1.6	79.6	
WC	(A8)N1·HN3(T15)	2.2±0.3	3.4	1.7	94.7	53.3[a]
	(A8)N6H62·O4(T15)	2.8±0.8	4.7	1.6	53.4	
WC	(C9)O2·H22N2(G14)	2.2±0.3	3.5	1.6	95.4	49.5[a]
	(C9)N3·HN1(G14)	2.8±0.6	4.8	1.8	49.5	
	(C9)N4H41·O6(G14)	3.2±0.9	6.1	1.7	34.9	34.5[b]
WC	(G10)N2H22·O2(C13)	1.9±0.1	2.6	1.6	100.0	98.6[a]
	(G10)N1H·N3(C13)	2.0±0.2	3.4	1.7	98.6	
	(G10)O6·H41N4(C13)	2.4±0.2	4.8	1.7	84.2	84.2[b]
cs	(A4)N6H62^N1(A18)	4.2±0.9	7.4	1.9	7.8	
cs(ρ)	(BU6)O4^H61N6(A16)	3.9±0.9	6.8	1.8	10.2	
cs	(T7)O4^HN3(T15)	3.9±1.1	7.4	1.7	13.7	
cs(μ)	(T7)O2^HN3(T17)	5.2±0.9	8.3	2.1	0.4	
cs	(T7)O4^HN3(T17)	5.4±0.9	8.5	1.9	1.5	
cs	(A8)N1H^62N6(A16)	4.7±0.9	8.2	1.9	0.6	

[a] Two canonical WC, or wb H-bonds
[b] Three canonical WC H-bonds

groove as deeply as sterically allowed. This penetration is accompanied by distortions of the DNA backbone and eventually opening of the minor groove. With the elapse of MD time, as exemplified in Fig. 11, and when e_{aq}^- moves away, the abnormalities are generally repaired, while counter ions are rearranged.

Discussion

The present study of the wobble $(\mathrm{BUdR{\cdot}T})-\mathrm{DNA}-e_{aq}^-$ system is a continuation of our previous report [24], which described the dynamics and interactions of e_{aq}^- with a normal BUdR·A-substituted DNA duplex. Although many of the dynamics features of e_{aq}^- and DNA are similar, there are differences, which can be assigned exclusively to the altered DNA dynamics due to the presence of the mismatched base pair.

Motion of e_{aq}^- and close contact sites with w-DNA

The overall motion of the electron resembles that in n-DNA, as generally represented by the corresponding XYZ_Abs(e_{aq}^-) plots. As in n-DNA, the longer quasi-linear segments (Fig. 1) are associated with unperturbed motion, usually along the DNA major groove cleft. In both cases, the $^-(H_2O)_6$ cluster structure was intact, showing similar average degrees of deformability, $\mathrm{DEF_{ABS}}(e_{aq}^-)$ (3.1 Å vs 3.0 Å) and almost equal $\mathrm{R_{GYR}}(e_{aq}^-) = 2.28$ and 2.26 Å (for w-DNA and n-DNA, respectively). Most importantly, the diffusion coefficients, $\mathrm{D}(e_{aq}^-)$, were practically the same, 3.8×10^{-9} and 3.9×10^{-9} m s^{-2} for w-DNA and n-DNA, respectively. These data prove that both systems were uniformly treated and thermally equilibrated. However, and independently of the same starting geometry, several differences concerning e_{aq}^- dynamics are evident. Thus, the occupancy of the close-to-DNA space for

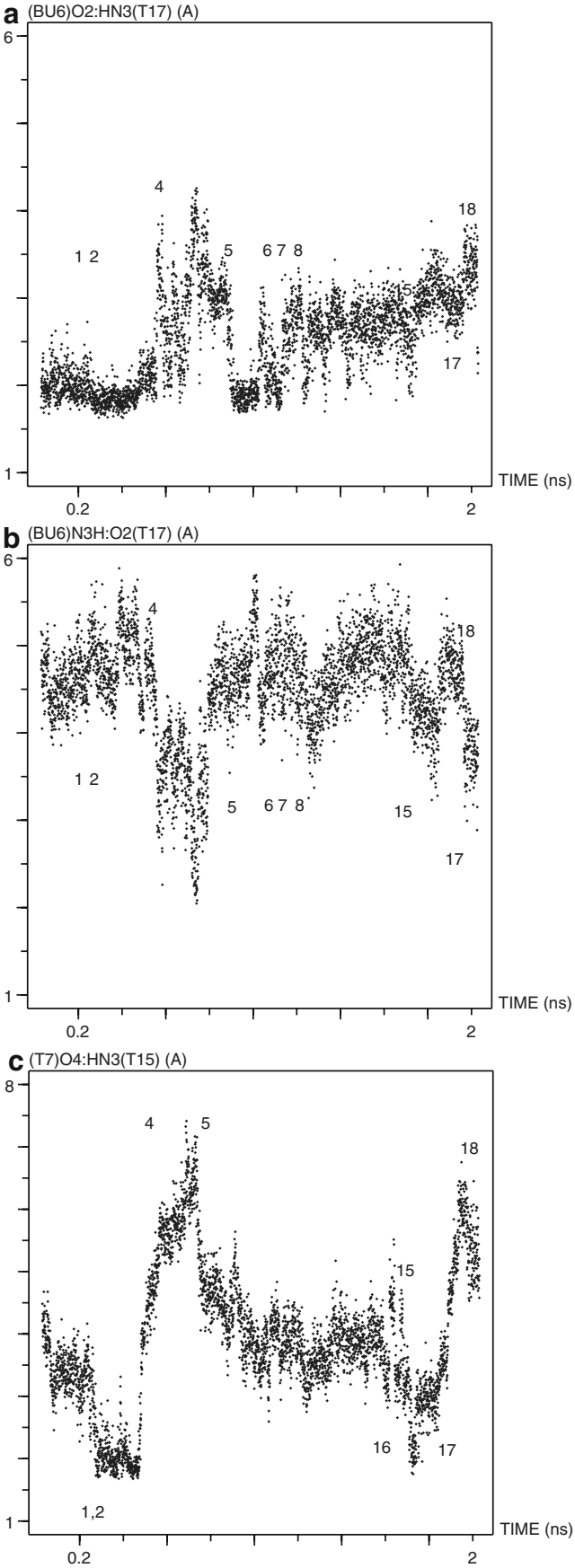

◀ **Fig. 9** H-bonding interbase distance-trajectories. **a** Oscillation pattern of wobble H-bonding between (BU6)O2·HN3(T17) atoms. Presents a component of the full W↑(αβ) conformation denoted as W(β′); H-bonded ~47% of total time (Table 3). **b** Distance trajectory of (BU6)N3H·O2(T17), a component of the rare W↓(βα) conformation W(β″) and mirror image of **a**; H-bonded only ~1% of total time. **c** The trajectory of the cross-strand (cs) distance between O4(T7) and HN3(T15) atoms. The average unperturbed distance without e_{aq}^- is ~3.6 Å. The plot indicates short distances of potential cs H-bonding (~13.7% of total 2 ns MD time). Positions of some close interaction sites of e_{aq}^- with DNA are indicated as a reference

w-DNA and n-DNA (cut-off distance <5 Å) was 0.7% vs 1.6%, respectively (from a total of 4,000 MD configurations). Nevertheless, the electron interacted with larger number of individual bases in w-DNA. For instance, in n-DNA, the electron moved closely toward only 4 NBs, all from the non-brominated DNA strand, while in w-DNA 11 NBs from both strands were found to come within reach of e_{aq}^-. At present, there is no apparent explanation for this disparity, other than the different dynamic structure of the isosteric DNA sequences under study. Notably, bromouracil (BU6), incorporated in both DNA duplexes, was approached by e_{aq}^- several times in w-DNA only (Table 2). The latter finding is relevant to the reported enhanced BUdR e_{aq}^--

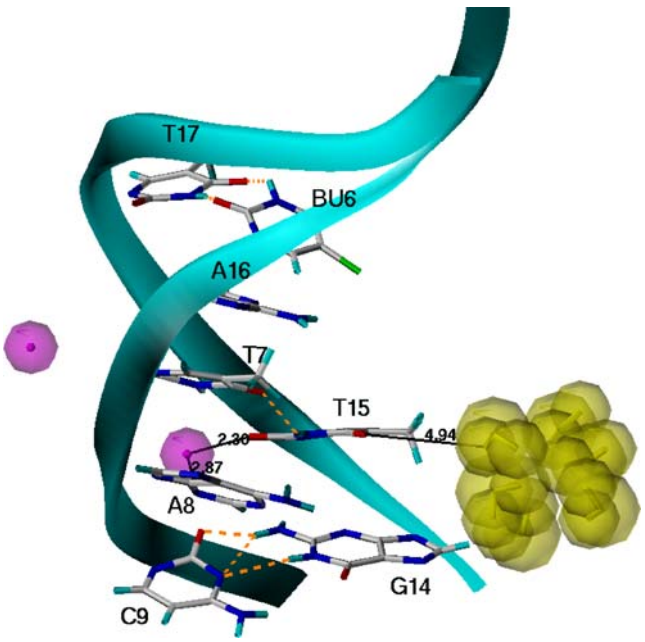

Fig. 10 Perturbation of DNA structure (Site-2, backbone as *cyan* ribbon). The electron in *yellow space-fill* interacts with the O4(T15) atom at a distance of 4.94 Å; BU6·T17 and C9 ·G14 are correctly paired. *Orange dashed lines* H-bonds. The two base pairs in the middle, T7**:**A16 and A8**:**T15, are disoriented, presenting a zipper-like structural motif. *Orange dashed line* cs-contact, (T7)O4^HN3(T15). The structure is locked by a minor groove-infiltrated Na^+ ion (ID706, *lower right magenta sphere*) at distances of 2.30 Å and 2.87 Å to O2 (T15) and N3(A8), respectively. A nearby Na^+ (*upper left magenta sphere*) occupies a normal position within the minor groove

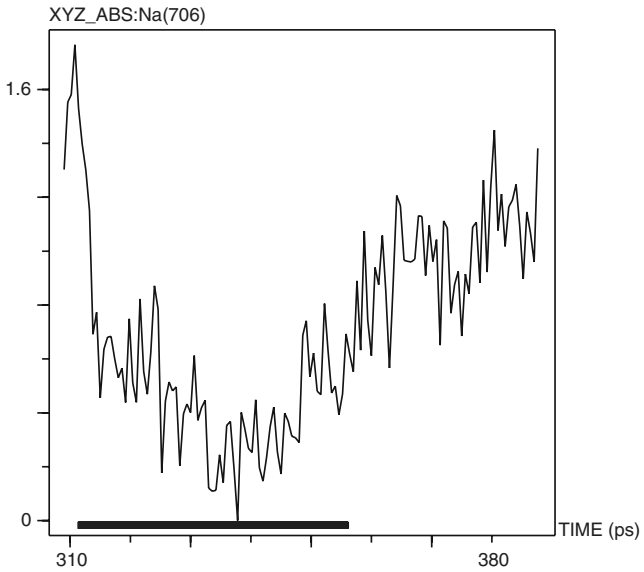

Fig. 11 Translocation of the Na^+ ion (ID706) from a near-PO position deeper into the minor groove concerted with the e_{aq}^- advancement towards T15 from the major groove side (Site-2). An 80 ps XYZ_ABS trajectory segment is shown; reference coordinates are from the configuration of the closest contact of e_{aq}^- with C5M(T15), which coincides with the deepest Na^+ penetration (Fig. 10). *Bar* Approximate e_{aq}^- residence time at this close-to-DNA location

radiosensitisation efficiency of wobble (bulged) vs normal Br-substituted DNAs [25–27]. Additionally, in w-DNA, all interactions with NBs were water-mediated, while in n-DNA a direct NB–e_{aq}^- interaction (H-bonding) has been identified [24].

Water dynamics and the formation of a shared hydration shell between DNA and e_{aq}^-

Notwithstanding the above differences, the overall pattern of recruitment of bulk water in the "second" aqua-shell by the $^-(H_2O)_6$ cluster, and the structured water involved in the DNA–e_{aq}^- interactions were analogous in the w-DNA and n-DNA systems. The results from this study confirm that stronger (longer) e_{aq}^- immobilisation in sites of close approach to DNA, depends on the more robust H-bonding network that involves the single-shared tightly packed hydration water layer between e_{aq}^- and DNA (Figs. 3b, 4). Since the dynamics of the build up of the shared hydration layer is presumably also important in CT to DNA, here we presented a deeper insight into this concerted process (Figs. 5, 6). In particular, following a multi-step e_{aq}^- reorientation, a bulk water molecule could be recruited by the electron and subsequently transferred to the DNA hydration layer, where it would remain immobilised disengaging the electron from the DNA. The dynamic scale of this process is a few picoseconds. We also estimated the self-diffusion constant of unbound water, $D(H_2O) = 2.1 \times 10^{-9}$ m^2 s^{-1} (Table 1). The TIP3P water diffusion constant at 300 K reported by Essmann et al. [32] is in the range of $(5.1–5.8) \times 10^{-9}$ m^2 s^{-1} (under different treatment of Coulomb interactions). When compared with our results at 250 K, and assuming the validity of Fick's law in low-temperature/microheterogeneous media, using Stoke's formula, $D = RT/(6\pi r N_A \eta)$ one obtains $\eta \sim 2.0$ cP, which is in close agreement with the viscosity of pure water (≥1.85 cP) in ice. Likewise, our calculations give $D(Cl^-) = 1.3 \times 10^{-9}$ m^2 s^{-1} , which falls within the range of the experimental data [33], assuming $\eta \sim 2.0$ cP. Importantly, the computed mobility of e_{aq}^- under the present simulation conditions is larger by a factor of ~3 than the diffusion constant of a typical bulky halide ion, e.g. Cl^-, which again is in agreement with previous theoretical (QMD and MM) estimates [14, 34].

w-DNA dynamic structure

We examined the structure and dynamics of an 11-mer w-DNA duplex incorporating a BU·T mismatched pair and in the presence of e_{aq}^-. Previously, some dynamic properties of the same DNA, but in the absence of the mismatch and/or the electron have been reported [24, 28]. Known structural features of pyrimidine mismatched DNAs, especially in AT-tracts, include a decrease of the C′–C′ distances by ~1 Å and narrowing of the minor groove at the TT and BUT sites. The exposure of wobble-pair pyrimidine carbonyl groups into the DNA grooves results in excess solvation of the mismatched pairs [31]. In addition, wobble T·T (and BU·T) pairs do not stack entirely on either of their 5′-partners, but instead nearly halfway between the two. Together with the narrowing of the minor groove, this brings the opposite strands into close proximity and represents cs stacking and cs H-bonding [28, 31]. In this study, both the all-atom mass-weighted (mw)-RMSD trajectory plot (Fig. 8), and the time-averaged structure calculated in reference show a good agreement with the starting B-DNA, as confirmed by the RMSD values of ~ 2 Å, which are typically observed in MD simulations without [35] or with incorporated base mismatches [31, 36]. As can be seen from the trajectories in Figs. 8 and 9, the close approach of e_{aq}^- to DNA, and especially the longer-lived sites, e.g. no. 2, 5, 8, 18, etc., can be implicated in the abrupt DNA structural deviations (fluctuations). Overall, backbone atoms RMS displacement was somewhat higher than that of base atoms, in agreement with earlier findings [37]. Transient distortions of the backbone were observed only within the proximity of the sites of e_{aq}^- approach. For example, during the time-window between 500–900 ps, characterised by the lowest population of e_{aq}^-–DNA contact sites, the RMSD trajectory shows steady and low

DNA structure deviations (Fig. 8). Likewise, NB displacement appears dependent on the close presence of the negatively charged e_{aq}^-, coupled with counter ion translocation in the minor groove, and probably dynamic rearrangement of the DNA hydration layer. The local perturbations of the w-DNA duplex in the presence of e_{aq}^- encompass deviations from the canonical WC H-bonding pattern and formation of cs base contacts (potential non-canonical H-bonding) (Figs. 9, 10). In the presence of e_{aq}^-, the predominant wobble conformation is W↑(αβ), as it is without the $^-(H_2O)_6$ cluster [28]. It is difficult to judge if there is a correlation between W↑(αβ) vs the W↓(βα) exchange with the e_{aq}^- approach to DNA, since the wobble exchange is an intrinsic property of the mismatch. However, it is evident that the close presence of e_{aq}^- provokes dynamic instability and fluctuations in the BU6 and T17 orientation (Fig. 9a,b). The incorporated mismatched pair alters the dynamics of the neighbouring bases due to incomplete 5′-stacking and other phenomena [28, 29, 31]. In the present structure, the most perturbed is the T5·A18 pair (Table 3), which is upstream of the mismatch. While some of the structural deviations are similar to those observed with n-DNA [24], and might be specific for the five base-pair AT-tract sequence [28], others are unique and arise unambiguously from the altered wobble dynamics due to the mismatched base pair BU6·T17. The essential difference between n-DNA and w-DNA structural dynamics is the formation of cs base contacts in the latter. The cs-contacts are common for this wDNA duplex and exist without e_{aq}^-, i.e. cs(ρ) and cs(μ) [28], Table 3. However, at least three new cs-contacts were identified, which were formed only when e_{aq}^- was present. One of these, (T7) O4^HN3(T15), is particularly long-lived (>200 ps), and the trajectory plot shown in Fig. 9c suggests that the e_{aq}^- occupation of, e.g., sites-2,4,15–18 provokes displacement of the underlying nucleotide (in opposite directions). The e_{aq}^- approach to selected DNA sites is associated with deviations from the overall canonical WC w-DNA structure. These structural distortions correspond to a concerted base displacement, so that short duplex segments are arranged in zipper-like structures (Figs. 7, 10). However, in contrast to [36], the "zipper-partners" in the present case do not necessarily involve only the mismatched bases, but also normal flanking base pairs. Finally, and similar to n-DNA [24], it is evident that the electrostatic attraction of Na^+ ions (in the minor groove) by $^-(H_2O)_6$ located in the major groove is one of the reasons for the induction of backbone structural deformations. Direct cation-base interactions in mismatched DNA duplexes (e.g. in zipper core segments) are common [36]. Partial counter-ion penetration into the first and second minor groove hydration-layers of AT-tract DNA has also been observed experimentally [38]. In our studies with n-DNA and w-DNA in the presence of e_{aq}^-, when the electron moved away from the encounter sites, the backbone deformations due to the unusual Na^+ localisation were in general repaired. However, the systems clearly retained some "memory" of the configurations of close e_{aq}^- approaches (Fig. 7). The evidence found in this study suggests that the lag in backbone reparation is due to the relatively slow release of Na^+ ions trapped deep in the minor DNA groove (Figs. 10, 11).

Conclusions

The results from this study underscore the differences in the structural dynamics of normal and wobble BUdR-substituted DNA and their interactions with the hydrated electron. A significant dissimilarity of the e_{aq}^- approach to n-DNA and w-DNA bases was found. In particular, e_{aq}^- interacts with bromouracil in w-DNA, but not in n-DNA. The reasons for these differences likely depend not only on the DNA dynamic structure (per se), but also involve specific concerted rearrangements within the Debay-Hückel hydrated layers around the two DNAs. For the pertinent use of BUdR to enhance e_{aq}^--mediated radiation damage of DNA in the radiotherapy of cancer, it must be emphasised that w-DNA would be a more efficient target because: (1) the solvated electron interacts not only more frequently with pyrimidines (T and C) but also directly approaches BUdR, which has the highest EA; and (2) the dynamic structure of w-DNA is prone to frequent cs inter-base contacts (as without e_{aq}^-)—conditions expected to accelerate intra-DNA excess-electron (hole) CT between different nucleotides, thus leading to more extensive DNA damage, as observed experimentally.

Acknowledgement This work was supported by the Cancer Research Society (Canada).

References

1. von Sonntag C (2006) Free radical induced DNA damage and repair: a chemical perspective. Springer, Berlin
2. Fuciarelli AF, Sisk EC, Zimbrick JD (1994) Int J Radiat Biol 65:409–418
3. Wesolowski SS, Leininger ML, Pentchev PN, Schaefer HF (2001) J Am Chem Soc 123:4023–4028
4. Li X, Cai Z, Sevilla MD (2002) J Phys Chem 106:1596–1603
5. Wagenknecht H-A (2003) Angew Chem Int Ed Eng 42:2454–2460
6. Gaballah ST, Collier G, Netzel TL (2005) J Phys Chem B 109:12175–12181
7. Zimbrick JD, Ward JF, Myers LS (1969) Int J Radiat Biol 16:505–523
8. Cook GP, Greenberg MM (1996) J Am Chem Soc 118:10025–10030
9. Zheng Y, Cloutier P, Hunting DJ, Sanche L, Wagner JR (2005) J Am Chem Soc 127:16592–16598

10. Ito T, Rokita SE (2004) Angew Chem Int Ed Eng 43:1839–1842
11. Li X, Cai Z, Sevilla MD (2002) J Phys Chem 106:9345–9351
12. Boudaiffa B, Cloutier P, Hunting DJ, Huels MA, Sanche L (2000) Science 287:1658–1660
13. Clark T, Illing G (1987) J Am Chem Soc 109:1013–1020
14. Schnitker J, Rossky PJ (1989) J Phys Chem 93:6965–6969
15. Tauber MJ, Mathies RA (2003) J Am Chem Soc 125:1394–1402
16. Herbert JM, Head-Gordon M (2005) J Phys Chem A 109:5217–5229
17. Borgis D, Rossky PJ, Turi L (2006) J Chem Phys 125:064501-1–064501-13
18. Sommerfeld T, Jordan KD (2006) J Am Chem Soc 128:5828–5833
19. Shkrob IA, Glover WJ, Larsen RE, Schwartz BJ (2007) J Phys Chem A 111:5232–5243
20. Larsen RE, Schwartz BJ (2004) J Phys Chem B 108:11760–11773
21. Coudert F-X, Archirel P, Boutin A (2006) J Phys Chem B 110:607–615
22. Feng D-F, Kevan L (1980) Chem Rev 80:1–20
23. Kevan L (1981) Acc Chem Res 14:138–145
24. Gantchev T, Hunting DJ (2008) J Mol Model 14:451–464
25. Cecchini S, Girouard S, Huels MA, Sanche L, Hunting DJ (2005) Biochemistry 44:1932–1940
26. Cecchini S, Girouard S, Huels MA, Sanche L, Hunting DJ (2004) Radiat Res 162:604–615
27. Dextraze M-E, Wagner RJ, Hunting DJ (2007) Biochemistry 46:9089–9097
28. Gantchev TG, Cecchini S, Hunting DJ (2005) J Mol Model 11:141–159
29. Gervais V, Cognet JAH, Le Bret M, Sowers LC, Fazakerley GV (1995) Eur J Biochem 228:297–290
30. Schmidt KH, Han P, Bartels DM (1995) J Phys Chem 99:10530–10539
31. Sherer C, Cramer CJ (2004) Theor Chem Acc 111:311–327
32. Essman U, Perera L, Berkowitz ML, Darden T, Lee H, Pedersen L (1995) J Chem Phys 103:8577–8593
33. Lide DR (ed) CRC handbook of chemistry and physics, 73rd edn. CRC, Boca Raton
34. Koneshan S, Rasaiah JC, Lynden-Bell RM, Lee SH (1998) J Phys Chem B 102:4193–4204
35. Beveridge DL, Barreiro G, Byun KS, Case DA, Cheatham TE, Dixit SB, Giudice E, Lankas F, Lavery R, Maddocks JH, Osman R, Seibert E, Sklenar H, Stoll G, Thayer KM, Varnai P, Young MA (2004) Biophys J 87:3799–3813
36. Špačková N, Berger I, Šponer J (2000) J Am Chem Soc 122:7564–7572
37. Goodfellow JM, Cruzeiro-Hansson L, de Souza N, Parker K, Sayle T, Umrania Y (1994) Int J Radiat Biol 66:471–478
38. Shui X, Sines CC, McFail-Isom L, VanDerveer D, Williams LD (1998) Biochemistry 37:16877–16887